RSC Advances

PAPER

View Article Online
View Journal | View Issue

Cite this: *RSC Adv.*, 2023, **13**, 26839

Adsorption isotherms and kinetics for Pb(II) ion removal from aqueous solutions with biogenic metal oxide nanoparticles†

Anastassiya A. Mashentseva,[ab]* Nurzhigit Seitzhapar,[ab] Murat Barsbay,[c] Nurgulim A. Aimanova,[a] Assel N. Alimkhanova,[ab] Dmitriy A. Zheltov,[a] Alisher M. Zhumabayev,[ab] Bakhtiyar S. Temirgaziev,[d] Alimzhan A. Almanov[ab] and Daniyar T. Sadyrbekov[d]

This study investigates the sorption removal of lead(II) ions using zinc oxide (ZnO) and copper(II) oxide (CuO) nanoparticles synthesized through a wet burning method with the aid of plant extract from *Serratula coronata* L. The effect of plant collection time on polyphenol content was investigated and optimal conditions were determined. The structural and chemical properties of the nanoparticles were studied by scanning electron microscopy, energy dispersive analysis, X-ray phase analysis, and X-ray photoelectron spectroscopy. A comparative analysis of lead ion sorption on the surface of synthesized nanoparticles was conducted. The kinetic study revealed that the sorption process follows a pseudo-second-order mechanism, and the Freundlich sorption model provides a better fit for the experimental data. ZnO and CuO nanoparticles exhibited significant sorption capacities, with values of 163.6 and 153.8 mg g^{-1}, respectively.

Received 7th August 2023
Accepted 24th August 2023

DOI: 10.1039/d3ra05347d

rsc.li/rsc-advances

1. Introduction

The rapidly developing nanotechnology and the increasing utilization of nanoscale materials in biological and medical applications have spurred significant interest in the advancement and enhancement of methodologies and technologies in this field. Notably, researchers have focused on green chemistry methods, which rely on highly efficient, cost-effective, and non-toxic biological resources for the synthesis of metal nanoparticles and their oxides.[1,2] In contrast to conventional synthesis techniques, green chemistry approaches not only prioritize environmental friendliness, but also enable the synthesis of nanoparticles devoid of trace impurities associated with the use of traditional precursors and reducing agents.[3,4]

Among the variety of metal nanoparticles (NPs) obtained using plant extracts, nanoparticles of Cu, Ag, Co, Ni and oxides such as CuO, ZnO, NiO, Fe_3O_4 have garnered significant research attention due to their straightforward synthesis techniques and distinctive dimensional physicochemical properties.[5,6] These NPs hold immense potential for biomedical application[7,8] as well as various fields of materials science.[9–11] Additionally, they find extensive use as effective catalysts and sorbents for wastewater remediation, targeting diverse classes of pollutants such as nitrophenols, organic dyes, pesticides, pharmaceuticals, and others.[12–14] Among the aforementioned persistent pollutants, the presence of heavy metals in water poses a substantial global concern due to their significant contribution to environmental degradation.[15] Contaminated drinking water containing heavy metals such as arsenic, cadmium, nickel, mercury, chromium, zinc, and lead has emerged as a major health concern for the public and health care professionals alike.[16,17] According to the Environmental Protection Agency (EPA), heavy metal ions are designated as priority pollutants, necessitating their elimination or reduction from any water bodies that may or may not interact with the environment.[18,19] The accumulation of heavy metals in living systems without degradation leads to harmful levels of exposure, while heavy metal waste pollutes water and soil surfaces, posing adverse effects on the health and continuity of all living species.[17,20]

A diverse array of conventional techniques has been employed for the removal of heavy metal ions from water, and several of these methods, such as precipitation, ion-exchange, reverse osmosis, membrane separation, have already demonstrated successful results.[21,22] Among these approaches, adsorption stands out as one of the most promising and widely used methods due to its simplicity of operation, high efficiency,

[a]*The Institute of Nuclear Physics of the Republic of Kazakhstan, 050032 Almaty, Kazakhstan. E-mail: a.mashentseva@inp.kz*

[b]*Department of Nuclear Physics, New Materials and Technologies, L.N. Gumilyov Eurasian National University, 010008 Astana, Kazakhstan*

[c]*Department of Chemistry, Hacettepe University, 06800 Ankara, Turkey*

[d]*NPJSC E.A. Buketov Karaganda University, 100024 Karaganda, Kazakhstan*

† Electronic supplementary information (ESI) available. See DOI: https://doi.org/10.1039/d3ra05347d

and economic benefits. Recently, there has been considerable interest in exploring the potential of biogenic nanomaterials as effective sorbents for the removal of heavy metal ions.[23,24] Various plant sources, including extracts from leaves, flowers, seeds, fruits, peels, and roots, have not only been extensively utilized for the synthesis of NPs but also hold promise as supporting materials for biogenic composites.[25]

The Republic of Kazakhstan boasts a rich flora, with over 200 endemic plants. Among these is *Serratula coronata* L. CR (SCR), a forest-steppe species belonging to the Asteraceae Dumort family, which is widely distributed in Eastern Europe, Western Siberia, Central and Northern Kazakhstan.[26] The aerial part (leaves, stems) of SCR, found in Central Kazakhstan (Karaganda region) exhibits a significant enrichment of various phytoecdysteroids and flavonoids.[27–29] Notably, the phytoecdysones derived from SCR promise as potential agents for the treatment of different skin diseases,[30–32] while flavonoids demonstrate noteworthy antioxidant activity.[33] Despite the abundant presence of secondary metabolites in SCR, which are known to be capable of reducing metal ions, this plant remains relatively understudied as a potential precursor for the biogenic synthesis of catalytically active metal oxide nanoparticles.[34,35]

In recent studies, various biogenic nanomaterials have been explored for the removal of lead (Pb) ions, yet the utilization of indigenous plant sources to develop environmentally friendly wastewater treatment technologies remains a pressing objective for every nation. This study aims to provide essential insights into the optimal conditions for the collection and extraction of SCR, and subsequently, to investigate the efficacy of biogenic ZnO and CuO nanosized adsorbents in the removal lead(II) ions from aqueous media under bath mode conditions. A comprehensive analysis of the physical and chemical properties of the NPs will be undertaken, and a thorough investigation of the kinetics and equilibrium sorption of Pb(II) ions will be conducted.

2. Materials and methods

2.1. Materials

Copper nitrate, zinc nitrate, quercetin, rutin, acetonitrile obtained from Sigma Aldrich (h.d.a.) were used without additional purification. Ethanol (96.2%) was purchased from Talgar-Alcohol LLP. The preparation of the Pb(II) feed solution was accomplished using the state standard sample (SSS) of Pb(II) (Ekroschem, St. Petersburg, Russia). Throughout all experiments, deionized water (18.2 Mohm cm^{-1}, Aquilon – D301, Aquilon JSC) was utilized.

2.2. Collection and treatment of plant materials

The collection of SCR plant material was conducted during the vegetation phase, spanning from mid-May to mid-July 2021, encompassing the period from the onset of vegetation to the budding phase of the plant. The collection area for the raw material was located in Spasskie Sopky of the Abay district of the Karaganda region, situated in the Central Kazakhstan region. The dry raw materials, consisting of buds, leaves and stems of SCR, were finely crushed to achieve a particle size of 2–3 mm. For each extraction experiment, a sample weight of 20 g was utilized. To maximize the extraction of polyphenolic components, various extractants were tested namely ethanol, 70% water–ethanol solution, and 0.1 M aqueous solution of sodium bicarbonate. In particular, a 70% (v/v) water–ethanol solution was employed based on previous findings, which demonstrated its ability to yield the highest quantity of flavonoids from plant raw materials.[36]

A pre-weighed sample of the plant material was placed inside a 250 mL round-bottom flask, which was equipped with a reflux condenser. The flask was then filled with the appropriate type of extractant. Subsequently, the flask was thoroughly mixed, and the mixture inside was heated using a mantle heater until the solvent reached its boiling point. The extraction process was allowed to proceed for a maximum duration of 3 hours. After completion of the extraction, the liquid extract was cooled to room temperature and then subjected to thickening through vacuum distillation following the filtration process. To ensure the most effective removal of any remaining extractant residues, the obtained extract was subjected to further evaporation in a water bath at a controlled temperature of 35–40 °C for a period of 6–7 h.

2.3. Study of the chemical composition of SCR extracts

The obtained samples were analyzed using reverse-phase High-Performance Liquid Chromatography (HPLC) conducted on a Shimadzu LC-20AD Prominence system. For the isocratic mode detection of quercetin and rutin, a mixture of 0.1% aqueous H_3PO_4 solution and CH_3CN (50 : 50, v/v) was used as the eluent. The flow rate was set at 0.5 mL min^{-1}, and 10 μL of the sample was injected. The column temperature was maintained at 40 °C, and a Promosil C18 column with dimensions 4.6 × 150 mm, particle size 5 μm, and 100 Å pore size from Agela Technologies (Ca, USA) was utilized. In the case of pinostrobin detection, a mixture of chloroform and acetonitrile in a 50–50% ratio was employed, following similar parameters as used for quercetin and rutin detection. To prepare each sample for analysis, it was dissolved in 200 μL of $CH_3CN : H_2O$ (50 : 50), sonicated at 30 °C, and then diluted with 1.6 mL of $CH_3CN : H_2O$ (50 : 50). Standard samples of rutin, quercetin, and pinostrobin (Sigma Aldrich) were used as reference standards, and their respective calibration curves are presented in Fig. S1.† The content of phenolic compounds in the extracts was determined spectrophotometrically using the Folin–Ciocalteu assay.[37,38] Calibration curves for standard substances such as caffeic acid, chlorogenic acid and gallic acid were constructed (Fig. S2†), allowing for the calculation polyphenol content in the SCR extract based on the equations derived from these curves. The results were expressed in equivalent units of standard substances per 1 mg of extractive substance.

2.4. Synthesis of biogenic nanoparticles

CuO and ZnO nanopowders were synthesized using wet combustion techniques:[39] SCL extract was mixed with corresponding inorganic salt and dissolved in 25 mL of water–

Table 1 Experimental details of the synthesis of biogenic metal oxide nanoparticles

	Synthesis conditions			
NPs	Used chemicals	Annealing temperature, °C	NPs yield, g	Ref.
ZnO	Plant extract: 1.0 g, $Zn(NO_3)_2 \cdot 6H_2O$: 4.02 g, water–ethanol mixture: 25.0 mL	600	3.77	34
CuO	Plant extract: 3.07 g, $Cu(NO_3)_2 \cdot 6H_2O$: 12.3 g, water–ethanol mixture: 25.0 mL	500	3.97	35

ethanol mixture under constant stirring, then the solution was placed in a ceramic crucible in a muffle oven preheated to 200 °C for combustion for 3 min. The resulting mixture was filtered to remove ash from the plant extract and thoroughly washed several times with deionized water to remove any remaining impurities. On the final step the mixture was then annealed in a muffle oven at the predetermined temperature for 2 h. The specific synthesis conditions are provided in Table 1. The resulting fine powders were stored in an airtight container and directly utilized in the sorption experiments without any further purification.

2.5. Analysis of the structure and composition of biogenic nanoparticles

The morphology and dimensional characteristics of the nanoparticles were examined using a JEOL JFC-7500F scanning electron microscope (SEM) and a JEOL JEM-1400Plus transmission electron microscope (TEM). For elemental analysis, energy dispersive analysis (EDX) was conducted on a Hitachi TM3030 microscope, equipped with a Bruker XFlash MIN SVE microanalysis system, at an accelerating voltage of 15 kV.

The crystal structure of the nanoparticles was investigated using a D8 Advance diffractometer (Bruker, Germany) in the angular range of 2θ 30–80°, with a step size of $2\theta = 0.02°$ and a measuring time 1 s. The tube mode settings were 40 kV and 40 mA. The average size of crystallites was determined by analyzing the broadening of X-ray diffraction reflections using the Scherer equation.

For the X-ray photoelectron spectroscopy (XPS) measurements, a Thermo Scientific K-Alpha spectrometer (Waltham, MA, USA) was employed equipped with a monochromatized Al Kα X-ray source (1486.6 eV photons). Core-level spectra were recorded with a constant dwell time of 100 ms and pass energy of 30 eV, while survey spectra were obtained with pass energy of 200 eV. The step size for core-level spectra was 0.1 eV, and for survey spectra, it was 1.0 eV. The analysis chamber maintained a pressure of 2×10^{-9} Torr or lower. The binding energy (BE) values were referenced to the C 1s peak at 285 eV. Data processing was performed using Avantage software (version 5.41, 2019, Waltham, MA, USA).

The determination of the surface charge of the adsorbent based on the pH value was carried out by studying the pH_{PZC} (point of zero charge) value within the pH range of 3.0 to 9.0, following the method described in ref. 34. For this, 10 mL of a 0.01 M NaCl solution was adjusted to the desired pH value (pH_i) using 0.1 M HCl(aq) or NaOH(aq). Subsequently, 50 mg of ZnO NPs powder was added to each flask and shaken on a shaker for 12 h at room temperature. Afterward, the NPs were separated from the solution through filtration, and the final pH value (pH_f) of the resulting filtrate was measured.

2.6. Study of the process of sorption removal of Pb(II) ions using biogenic metal oxide nanoparticles

All experiments were conducted using batch equilibrium techniques. A feed solution of Pb(II) (100 ppm, pH 4.0) was prepared by diluting the certified Pb(II) reference solution (0.1 g L^{-1}, Ecroskhim, Russia). Disposable plastic vials (Isolab, Eschau, Germany) containing 15.0 mL of the solution and 50 mg of NPs powder were subjected to shaking (100 rpm) using IKA KS 3000 IS (IKA, Konigswinter, Germany) at room temperature for various durations ranging from 15 minutes and 10 hours. Each experiment was replicated three times. The concentration of Pb(II) in the aliquots was determined using ICP-MS (Thermo Fisher Scientific, XSeries 2, Bremen, Germany).

The quantity of Pb(II) adsorbed per unit mass of the sorbent (Q_e, mg g^{-1}) was determined using the eqn (1):[40]

$$Q_e = \frac{(C_0 - C_e) \times V}{m} \quad (1)$$

where C_0 is initial the feed concentration of Pb(II) (mg L^{-1}), C_e is the concentration of Pb(II) in the aliquots (mg L^{-1}), V is the volume of the solution (L), and m is the amount of NPs used (g).

The influence of pH on Pb(II) adsorption was studied within the pH range of 3 to 9, while keeping other parameters constant (initial Pb(II) concentration: 50 ppm, adsorbent dose: 50 mg, contact time: 300 min). The pH of the solution was adjusted dropwise using 1.0 M HCl(aq) or 1.0 M NaOH(aq). pH was measurements were performed using a digital pH meter, HANNA HI2020-02 (HANNA Instruments, Smithfield, VA, USA). All experiments were conducted in triplicate. Upon completion of the sorption process, the solution was decanted by centrifugation at 12 000 rpm, and the NPs were washed with deionized water, dried, and stored in a dry location.

3. Results and discussions

3.1. Determination of the optimal conditions for the preparation of SCR plant extracts

It is widely recognized that the content of biologically active components in plant extracts can vary significantly based on the extraction methods employed. Substances containing a hydroxyl groups in their composition tend to be slightly soluble or insoluble in aliphatic organic solvents, making it is more appropriate to use organic alcohols and their homologues for extracting cyclic alcohols.[41] An extensive review of the

literature indicates that for a more efficient extraction of the polyphenol fraction from plant materials, a multi-step extraction process is recommended. The initial phase involves using aliphatic saturated hydrocarbon solvents (such as petroleum ether and hexane), which facilitates the removal of non-polar component that are of limited practical and bioactive interest.[42] Subsequently, the next extraction step should employ solvents of higher polarity than aliphatic ones, such as esters (*e.g.*, ethyl acetate, butyl acetate), to extract medium-polar secondary metabolites like terpenoids, carboxylic acids, and aromatic hydrocarbons. For the final stage of purification and removal of plant by-products, extraction with trichloromethane is recommended. This particular step effectively eliminates chlorophyll, thereby eliminating ballast substances and reducing barriers to the complete extraction of the target products.[43]

In our studies, we opted to use ethyl alcohol and its 70% aqueous solution as the extractants, considering that ethanol is one of the main universal food extractants utilized for the extraction of biologically active compounds found in plants.[44] Additionally, it is important to note that ethanol is comparatively less toxic to the human body compared to other organic solvents. For the purpose of conducting a comparative analysis of the polyphenol extraction efficiency from the studied plants, an alkaline solution of sodium bicarbonate (baking soda) was employed as an extractant. This choice was motivated by the widespread utilization of sodium bicarbonate in both food and household applications, rendering it a viable alternative option for extraction in our research.

As can be seen from the data presented in Table 2, the highest extraction efficiency by weight was achieved with aqueous ethanol solution (EtOH-70), while the lowest extract yield was obtained during extraction with 0.1 M $NaHCO_3$ solution, owing to the limited solubility of many lipophilic compounds in aqueous solutions of inorganic salts. Comparatively, extraction with ethanol resulted in a lower degree of separation of the slurry extract than with a water–ethanol mixture.

The concentration of flavonoids in the studied plant extracts was determined by HPLC *via* the method of absolute calibration peak area. This involved comparing the peak area of the analyte with the peak area of a standard analyte sample with a predeterminated concentration. Although the highest amount of slurry extract (*i.e.* the total extractable substances) was observed during the processing of plant materials harvested at the beginning of the budding stage, the content of flavonoids in this type of material was found to be the lowest, as shown by HPLC analysis. Previous studies have highlighted that the presence of a large number of flavonoids and phenolic compounds in the composition of plant raw materials influences their reducing properties during the synthesis of metal nanoparticles and their oxides.[45–47] Flavonoids, which exhibit proton-donor properties, along with phenolic compounds known for their metal ion chelating capabilities, have been shown to play a crucial role in reducing Cu^{2+} ions to metallic copper and copper(I) oxide. These compounds can then be oxidized to form CuO by thermal annealing.[35,48] A similar

Table 2 The extraction parameters of SCR at various collection times

Time of plant materials collection	Solvent	Extraction temperature, °C	Weight of final extract, g
Beginning of vegetation phase	EtOH	78.0	3.91
	EtOH : water (70 : 30)	80.0	5.70
	0.1 M $NaHCO_3$	101.2	2.63
Vegetation phase	EtOH	78.0	4.2
	EtOH : water (70 : 30)	80.0	5.66
	0.1 M $NaHCO_3$	101.2	1.86
Beginning of budding	EtOH	78.0	3.75
	EtOH : water (70 : 30)	80.0	6.27
	0.1 M $NaHCO_3$	101.2	2.58

Table 3 Content of flavonoids and phenolic compounds in *SCR* extracts

		Flavonoids content, mg g^{-1}			Phenolic compounds content, mg g^{-1}		
Time of collection of plant materials	Solvent	Quercetin	Rutin	Pinostrobin	Gallic acid	Protocatechuic acid	Caffeic acid
Beginning of vegetation phase	EtOH	2.77	0.60	0.10	0.038	0.062	0.034
	EtOH-70.0	**2.59**	**0.89**	**0.12**	**0.112**	**0.174**	**0.104**
	$NaHCO_3$	1.86	0.33	0.01	0.058	0.097	0.056
Vegetation phase	EtOH	2.01	0.45	0.29	0.110	0.188	0.112
	EtOH-70.0	0.02	0.06	0.00	0.032	0.052	0.028
	$NaHCO_3$	1.50	0.19	0.02	0.110	0.186	0.111
Beginning of budding	EtOH	0.32	0.00	0.00	0.110	0.187	0.112
	EtOH-70.0	0.67	0.04	0.00	0.117	0.199	0.119
	$NaHCO_3$	0.38	0.00	0.00	0.116	0.197	0.118

influence of flavonoids on the formation of ZnO nanoparticles has been described elsewhere.[49,50]

To determine the total amount of phenolic compounds and specific phenolic substances, such as phenolic acids, in plant materials, various spectrophotometric methods are utilized. The Folin–Ciocalteu method, initially developed by Folin and Ciocalteu and later modified by Singleton Rossi Jr, is commonly employed for analyzing phenolic compounds. This method relies on the reduction of phenols with a phosphomolybdic acid reagent. In an alkaline medium, phenolic compounds undergo oxidation, leading to the formation of superoxide ions, which, in turn, react with molybdate to produce molybdenum oxide MoO_4^+, exhibiting intense absorption at 725 nm.[38] In this study, the content of phenolic compounds in the extracts was determined in terms of equivalents of specific phenolic acids, namely gallic, protocatechuic, and caffeic acids. Calibration curves were plotted for each standard substance (Fig. S2†). Table 3 presents the data on the content of phenolic compounds in the extracts of SCR expressed in terms of mg per 1.0 g of raw material. As evident from Table 3, the most enriched extract of SCR with flavonoids and phenolic acids was prepared from the plants collected during the beginning of the vegetation phase (mid-May). This specific type of extract will be used in the subsequent experiments concerning the synthesis of ZnO and CuO NPs.

3.2. Study of the structure and composition of biogenic metal oxides nanoparticles

SEM images of the synthesized nanoparticles are presented in Fig. 1a and b. The microphotographs reveal the presence of not only spherical and cubic crystals but also small voids and pores in the test sample. The occurrence of these voids can be attributed to the emission of a significant amount of hot gases from the reaction mixture during the wet combustion synthesis.[51] The crystallites of ZnO and CuO nanoparticles are interconnected through pores of various sizes and shapes. The nanoparticle size was determined from electron micrographs with magnifications up to 100 000×, indicating an average size of 32 ± 8 nm for zinc oxide nanoparticles and 57 ± 12 nm for copper oxide nanoparticles. Transmission electron microscopy data (Fig. 1c and d) further validate the dimensional and geometric characteristics of the synthesized nanoparticles. The investigation of the chemical composition using energy dispersion analysis (inset in Fig. 1d and e) reveals the presence of carbon in the composition of nanoparticles, accounting for approximately 11.9 at% for ZnO and 8.8 at% for CuO. This observation supports the role of the organic extract of SCR as a stabilizing and reducing agent during the nanoparticle synthesis, consistent with previously reported findings.[52,53]

The X-ray diffractogram of ZnO nanoparticles (Fig. 1e) reveals distinct diffraction peaks corresponding to the ZnO phase at 2θ values of 32.54° (110), 35.58° (002), 38.86° (200), 40.43° (112), 48.57° (−202), 53.65° (020), 58.39° (202), 61.57° (−113), and 68.07° (113), in accordance with previous studies.[54–56] These identified planes closely match the JCPDS file (JCPDS: 01-007-2551), indicating the hexagonal wurtzite structure (symmetry group $P6_2mc$ (186)) of the ZnO nanoparticles. Similarly, the X-ray diffraction pattern of CuO nanoparticles (Fig. 1f) exhibits a series of diffraction peaks characteristic of the monoclinic structure of copper(II) oxide, located at 2θ values of 32.54°, 35.58°, 38.86°, 40.43°, 48.573°, 53.65°, 58.40°, 61.57°, 66.05°, 68.07°, 72.36°, and 75.16°, which were assigned to (110),

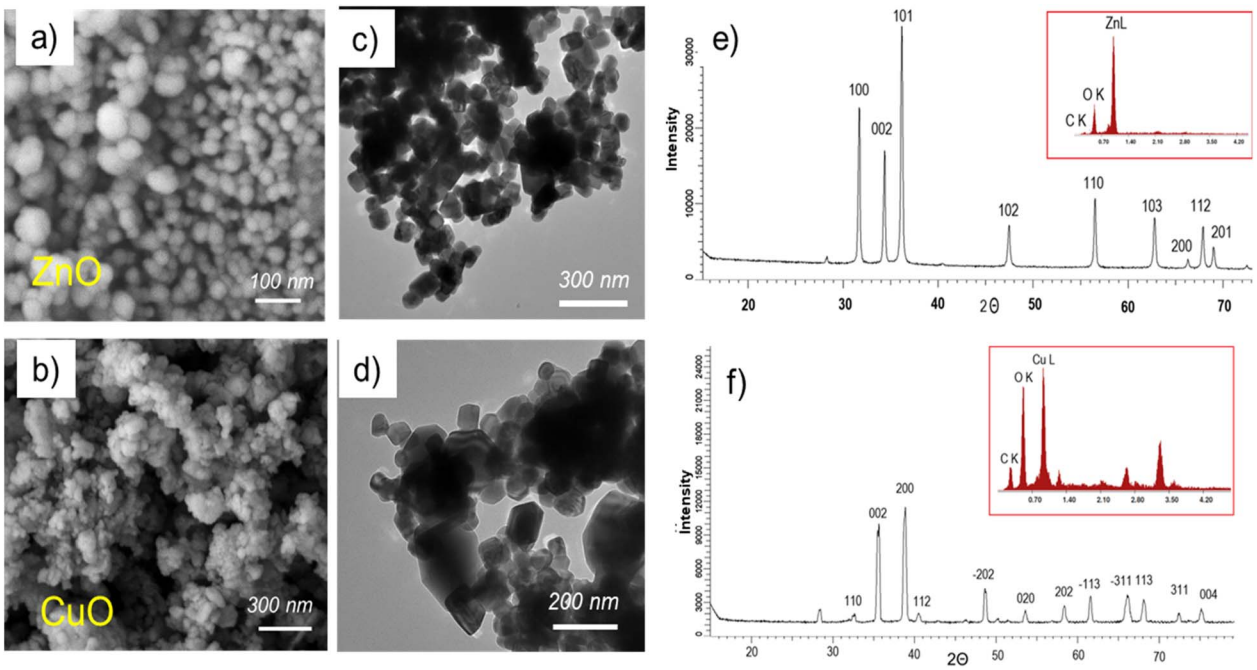

Fig. 1 Electron microphotographs of ZnO (a) and CuO (b) nanoparticle powders, TEM images of ZnO (c) and CuO (d) nanoparticles, X-ray diffraction spectra of ZnO (e) and CuO (f) nanoparticles.

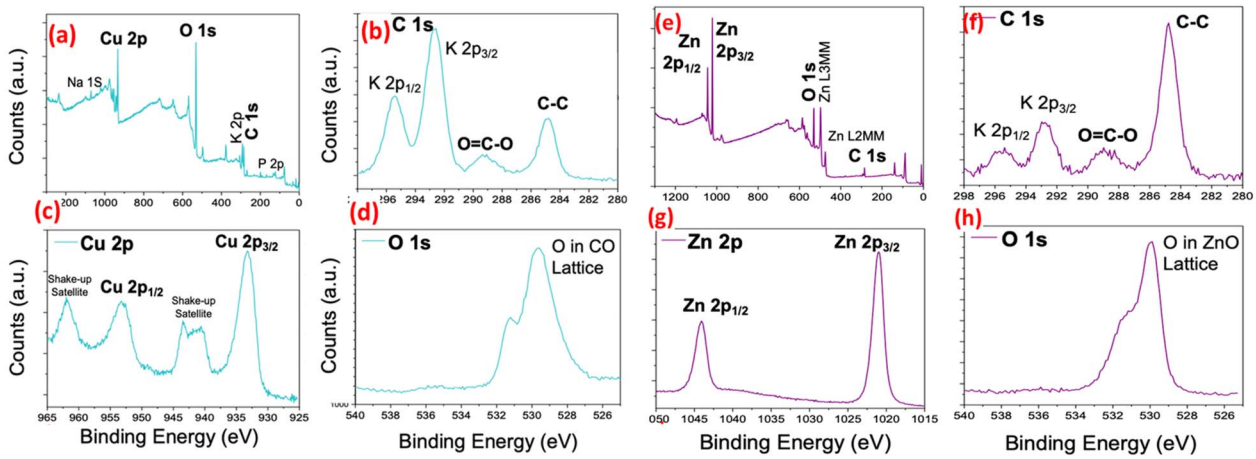

Fig. 2 Survey or wide energy range X-ray photoelectron spectroscopy (XPS) spectra of CuO (a) and ZnO (e), respectively. High resolution (core level) C 1s from as synthesized CuO (b) and ZnO (f) NPs, respectively, high resolution (core level) spectra of Cu 2p from as synthesized CuO. (c), high resolution (core level) spectra of Zn 2p from as synthesized ZnO (g) and high resolution (core level) O 1s from as synthesized CuO (d) and ZnO (h), respectively.

(002), (200), (112), (−202), (020), (202), (−113), (−311), (113), (311) and (004) respectively. No other characteristic peaks were observed except for those for CuO (JCPDS: 45-0937), indicating the as-obtained CuO NPs has high-purity.

The obtained X-ray diffraction spectra indicate the crystalline nature of the nanoparticles. The average size of CuO crystallites, calculated using the Scherer equation, was found to be 25.4 ± 3.9 nm, and for ZnO nanoparticles, it was 44.6 ± 5.9 nm. All synthesized nanoparticles demonstrated a high degree of crystallinity, with 84.0% for CuO nanoparticles and 91.2% for ZnO nanoparticles, as determined by approximating the values of the full width at half maximum (FWHM) lines using symmetric pseudo-Voigt functions.[57]

The wide energy range X-ray scans of each nanoparticle (Fig. 2) show that their chemical composition primarily consists of two basic elements, *i.e.* oxygen and the corresponding metal atom (Cu or Zn). In addition to these anticipated components, the presence of K and Cl elements is noteworthy, constituting about 5% of the composition, particularly in the case of CuO, where they are more prominent as impurities. These two elements also appear in the spectrum of ZnO, albeit in smaller quantities. The amount of carbon, a common element in both nanoparticle compositions, was determined as 9.1%, and 8.2% in the survey scans of CuO and ZnO, respectively. Furthermore, the high-resolution C 1s spectra of the as-synthesized CuO and ZnO exhibit a primary peak at 284.5 eV and another peak at a higher energy level around 288.1 eV. These C 1s peaks are commonly observed in XPS spectra on the surface of nearly all samples, attributed surface contaminations, and are referred to as adventitious carbon.[58–60] The C 1s peak component with a binding energy (BE) of 284.5 eV corresponds to C–C bonds, while the component at 288.1 eV is assigned to O–C=O bonds.[60] The detection of the C element in the XPS spectra of nanoparticles is a crucial finding, providing evidence for the involvement of organic residues from plant extracts in both formation and stabilization of nanoparticles. Furthermore, it aligns well with the earlier discussed EDX results.

The Cu 2p core-level XPS spectrum exhibits distinctive features that differentiate it from both Cu_2O and metallic Cu. Notably, dominant shake-up peaks are observed at the higher BE side of the Cu $2p_{3/2}$ and Cu $2p_{1/2}$ peaks, indicating the existence of an unfilled Cu $3d^9$ shell. This observation confirms the presence of Cu^{2+} in the CuO sample.[61,62] Moreover, the peaks at 953.9 eV and 933.4 eV in the core level spectra of Cu 2p can be assigned to Cu^{2+} $2p_{1/2}$ and Cu^{2+} $2p_{3/2}$ of CuO, respectively.[62] Additionally, the core-level XPS spectrum for O 1s in CuO nanoparticles reveals two components at approximately 529.1, 531.0 eV. The more intense peak at 529.1 eV is attributed to the binding energy of lattice oxygen in CuO lattice, consistent with the binding energy of O^{2-} ions in metal oxide sites (Cu^{2+}–O^{2-}).[62,63] The second peak at 530.78 eV can be assigned to the binding energy of oxygen defects/vacancies within the matrix of CuO.[57,62] These results align well with previous works[63,64] and provide strong evidence of the CuO structure. Similarly, the high-resolution XPS spectrum of the Zn 2p region in ZnO nanoparticles displays two fitting peaks located at approximately 1043.6 and 1020.5 eV, corresponding to Zn $2p_{1/2}$ and Zn $2p_{3/2}$, respectively.[34] Furthermore, the XPS spectrum of the O 1s region in ZnO nanoparticles shows an asymmetrical peak centered at about 529.6 eV. These results from the core-level Zn 2p and O 1s spectra are in good agreement with previous data and confirm the ZnO structure.[65,66] In conclusion, based on the discussed XPS data, the successful synthesis of both nanoparticle structures (CuO and ZnO) is confirmed, and the desired structures have been achieved.

3.3. Study of lead(II) ion sorption kinetics

The process of adsorption is inherently a time-dependent and is influenced by the physicochemical characteristics of the adsorbent materials involved. Fig. 3a illustrates the effect of pH

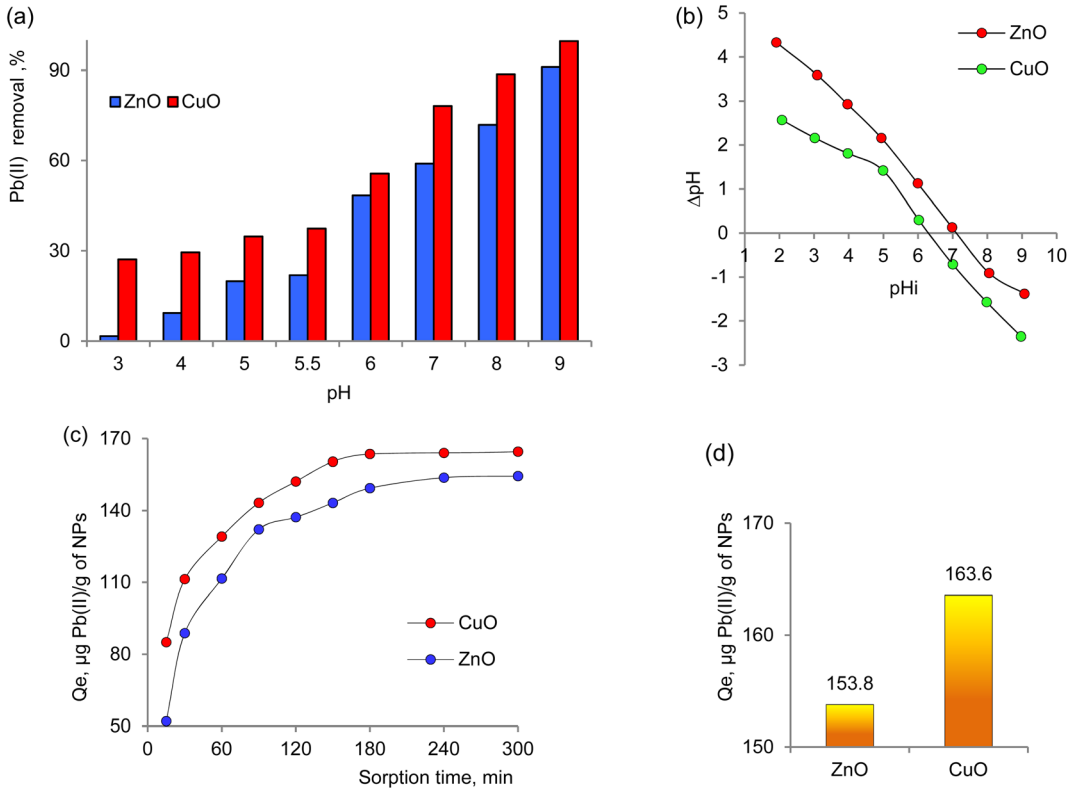

Fig. 3 The effect of pH on the sorption efficiency of lead ions (a), the graph depicting the zero charge point (pH_{PZC}) of the surface of the nanoparticles (b), the change in sorption capacity of nanoparticles with respect to sorption time (c), and the equilibrium sorption capacity of the studied sorbents (d).

on the adsorption of Pb^{2+} by biogenic nanoparticles within a pH range spanning from 3.0 to 9.0. The pH of the medium plays a crucial role in investigating sorbent properties and determines their reactivity. Moreover, the pH value directly impacts the state of the metal ions in solution, effectively regulating the sorption process. Efficiency of lead ion removal increases with the initial pH rising from 3.0 to 7.0. However, the limited efficiency of the studied sorbents in acidic conditions is attributed to the high concentration of H^+ ions, which compete with Pb^{2+} ions for available active sites on the adsorbent surface, significantly reducing their sorption capacity.[67,68]

At a pH of 5.5, the removal efficiency of Pb^{2+} by ZnO and CuO nanoparticles is found to be 21.9% and 37.4%, respectively. However, at a pH of 7.0, there is a notable increase in the sorption of lead ions by CuO, reaching 78.2% in the case of CuO. Nevertheless, several previous studies have shown that at pH levels above 6.0, additional deposition of Pb^{2+} ions occurs due to the formation of lead hydroxide, and at pH 9.0, nearly complete disappearance of Pb^{2+} ions in the solution is observed.[69,70] Therefore, conducting sorption tests at pH levels lower than 6.0 is deemed more appropriate.

The parameter known as pH zero charge point (pH_{PZC}) determines the pH at which the adsorbent's total surface charge becomes zero. The study of pH_{PZC} is important for revealing the adsorption mechanism and explaining the interactions between the sorbent and adsorbate.[71] Fig. 3b shows the relationship between pH_{final} on $pH_{initial}$, and the pH_{PZC} value obtained for biogenic ZnO NPs is approximately 7.1. This result indicates a positive surface charge under the conditions studied and agrees well with pH_{PZC} values reported in previous studies.[72–74]

Regarding the change in the sorption capacity of nanoparticles over time (Fig. 3c), it was observed that biogenic CuO NPs reach saturation after 180 minutes of sorption, while ZnO NPs reach saturation later, after 240 minutes. Subsequently, the equilibrium sorption capacity (q_e) for Pb(II) sorption from a solution with a concentration of 50 ppm was deduced based on the experimental data (Fig. 3d).

For a comprehensive understanding of the adsorption mechanism of new sorbents, kinetic studies are of paramount importance kinetic studies of paramount importance. In this study, we used three kinetic models to predict the kinetics of Pb(II) adsorption on bigenic NPs. The models used were the pseudo-first and pseudo-second order, as well as the Elovich model.[75–79] The pseudo-first-order rate model, originally proposed by Lagergren,[80] is among the early models of sorption kinetics, focusing on sorption capacity and describing sorption from a liquid medium by solid sorbents. The linear form of the pseudo-first-order model is provided in Table 4. From the graphical relationship $\ln(q_e - q_t) = f(t)$ (Fig. 4a), the values of k_1 and the correlation coefficient R^2 were determined and are listed in Table 1. However, it is important to note that the observed low correlation coefficient value for the pseudo-first-order

Table 4 Comparison of the parameters of different kinetic models for describing the sorption of Pb(II) using biogenic metal oxide NPs

Kinetic model	Linear equation of the kinetic model	Parameters of the kinetic model	Sorbent	
			CuO	ZnO
Pseudo-first order	$\ln(q_e - q_t) = \ln q_e - k_1 t$	k_1, min^{-1}	0.024	0.017
		q_e, mg g^{-1}	137.3	118.2
		R^2	0.95	0.98
Pseudo-second order	$\frac{t}{q_t} = \frac{1}{k_2 q_e^2} + \frac{t}{q_e}$	$k_2 \times 10^{-4}$, g mg^{-1} min^{-1}	1.97	2.09
		q_e, mg g^{-1}	178.57	169.49
		R^2	0.99	0.99
The Elovich model	$q_t = \frac{1}{\beta}(\ln \alpha\beta) + \frac{1}{\beta}\ln t$	α, mg g^{-1} min^{-1}	0.081	0.084
		β, mg min^{-1}	0.038	0.031
		R^2	0.95	0.95

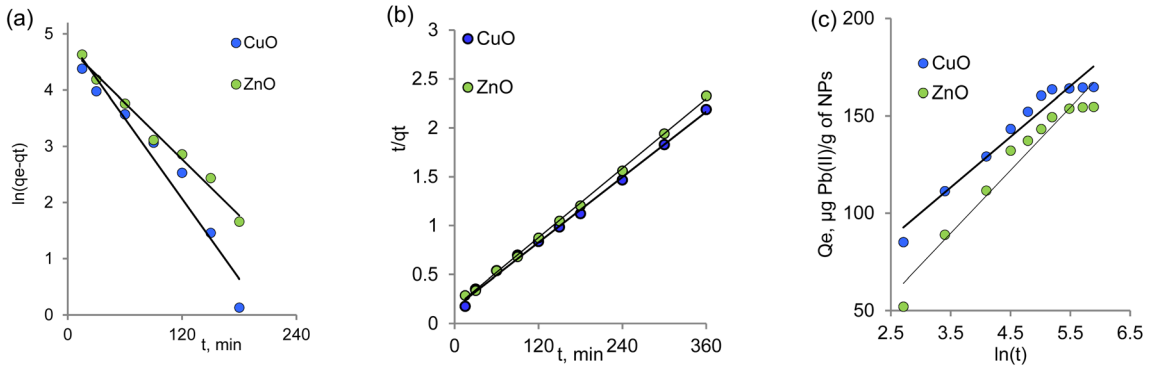

Fig. 4 Kinetics of Pb(II) sorption by biogenic NPs according to the pseudo-first (a), pseudo-second (b), and the Elovich (c) kinetic models.

kinetic model suggests that the kinetics of Pb(II) adsorption by the biogenic nanoparticles of metal oxides obtained do not conform to the pseudo-first-order kinetic model. Therefore, further investigation and application of alternative kinetic models are necessary to elucidate the kinetics of the sorption process accurately.

To describe the sorption process, it is believed that the first-order kinetic model is applicable at the initial stage, where the concentration of sorbate ions reaching the functional groups of the sorbent is significantly lower than the active centers of the sorbent.[81] Consequently, the order of the reaction can be mathematically reduced by incorporating the concentration of functional groups of the sorbent into the reaction rate constant. However, at later stages of the sorption process, the reaction rate is affected by the product of the concentrations of both components of both components, leading to a formal reaction order of two.[82]

A pseudo-second-order equation is considered suitable for describing the sorption process if the reaction between the adsorbate and the functional groups of the adsorbent proceeds strictly stoichiometrically, where one metal ion occupies one sorption position.[83] This model shares similarities with the pseudo-first-order kinetics model but is more comprehensive in describing the entire sorption process.

The rate constant k_2, the value of q_e, and the corresponding linear regression correlation coefficient R^2 were calculated from the linear plot of the dependence $t/q_t = f(t)$ as shown in Fig. 4b and are presented in Table 4. The calculated q_e values for ZnO and CuO were 169.45 and 178.57 mg g^{-1}, respectively, and in agreement with the experimental data (Fig. 3g) for the pseudo-second-order kinetics.

The pseudo-second-order equation accounts not only for sorbate–sorbent interactions but also for the intermolecular interactions of the adsorbed substances. On the other hand, the Elovich model considers the contribution of both sorption processes and desorption phenomena to the kinetics of substance extraction, with desorption gaining significance as equilibrium is approached.[84] The kinetic parameters of the Elovich model were calculated from the linear dependence of q_t on $\ln(t)$ (Fig. 4c) and are provided in Table 4. Higher values of α compared to β indicate a faster absorption rate compared to lead ions' desorption.[85]

The correlation coefficient values (R^2) indicate that the most appropriate description of the sorption of lead(II) ions on the studied sorbents is achieved using the pseudo-second order model. This is evident from the linear nature of the graphical dependencies of this model in Fig. 3b, which remains consistent throughout the entire time interval. The applicability of the pseudo-second-order model to the biogenic sorbents suggests that the chemisorption stage governs the limiting step of the process, with the influence of the diffusion stage being insignificant.[86]

3.4. Study of the Pb(II) sorption mechanism

Intensive studies on the toxic pollutant migration in aquatic environments and the development of new removal methods have contributed significantly to the advancement of adsorption methods. A profound understanding of adsorption equilibrium is essential for comprehending the adsorption process accurately. Adequate interpretation of adsorption isotherms is crucial for refining the adsorption mechanism pathways and designing efficient adsorption systems.[87] In this context, the section focuses on the applicability of various models to interpret experimental data on the adsorption of Pb(II) ions by biogenic nanoparticles under investigation, aiming to identify the most suitable model for describing the adsorption process.

Table 5 Parameters of adsorption isotherms for biogenic nanoparticles' sorption of Pb(II) ions

Isotherm	Linear equation	Parameter	Value	
			CuO	ZnO
Experiment		q_0, mg g^{-1}	163.6	153.8
Langmuir	$\frac{C_e}{q_e} = \frac{C_e}{Q_0} + \frac{1}{Q_0 b}$	Q_0, mg g^{-1}	84.8	80.0
		b, L mg^{-1}	2206.9	1353.6
		R^2	0.97	0.91
Freudlich	$\ln q_e = \ln k_F + \frac{1}{n}\ln C_e$	k_F, mg g^{-1}	387.5	235.4
		n	2.5	1.6
		R^2	0.99	0.99

According to Langmuir's adsorption theory, adsorption takes place on equivalent, localized active centers, with each center accommodating only one molecule. Saturation of adsorption occurs as these active centers become filled. The adsorbed molecules do not interact with one another and desorb after a certain time, establishing a dynamic equilibrium.[87,88] The linear form of the Langmuir adsorption isotherm equation, derived from molecular-kinetic theory and the concept of the monomolecular nature of the adsorption process, is presented in Table 5. The parameters b and Q_0 characterize the adsorbent–adsorbate pair. Fig. 5a illustrates the graph of the dependence $C_e = f(C_e/Q_e)$. The values of Q_0 and b were calculated from the slope and intersection of the lines on the graph in the corresponding coordinates of the linear isotherm equation, and are listed in Table 5.

The Freundlich model isotherm equation describes adsorption on a heterogeneous surface, where the adsorption centers possess varying energy levels. Initially, the active sorption centers with maximum energy become filled. Fig. 4b shows the

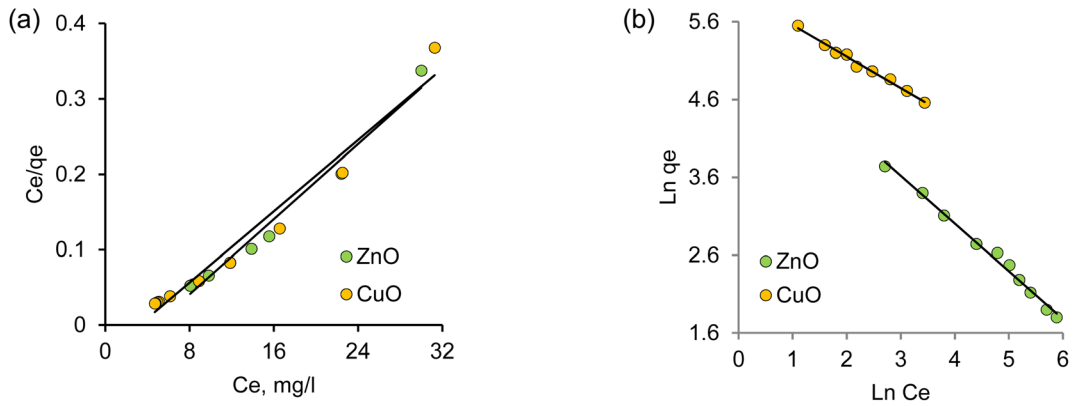

Fig. 5 Adsorption isotherms of Pb(II) on biogenic CuO and ZnO nanoparticles in linear coordinates of Langmuir (a) and Freundlich (b) isotherms.

Table 6 Sorption capacity of nanosized sorbents of lead(II) ions

Sorbent	Sorbent testing conditions						
	Initial sorbate concentration, mg L^{-1}	Sorbent weight, g	Aliquot volume, mL	pH	Q_e, mg g^{-1}	Rate constant k_2, g mg^{-1} min^{-1}	Ref.
CuO NPs (microwave synthesis)	50.0	0.1	50.0	—	125.0	0.0235	90
CuO NPs (magnetron sputtering)	1000.0	2.0	100.0	6.0	37.03	0.0054	91
CuO nanorods	1000.0	1.0	100.0	8.5	3.31	—	92
ZnO NPs (biogenic synthesis)	25.0	0.1	25.0	5.0	19.65	—	24
Magnetic NPs modified with chitosan	100.0	0.1	100.0	6.0	498.6	0.0002	93
Magnetic NPs Fe_3O_4, modified with polyethyleneimine	50.0	1.0	100.0	5.0	33.65	0.023	94
CuO NPs (biogenic synthesis)	50.0	0.05	15.0	5.0	163.6	0.00019	This
ZnO NPs (biogenic synthesis)					153.8	0.00021	study

experimental data on lead(II) ion adsorption in the linear Freundlich equation $\ln q_e = f(\ln C_e)$ coordinates. The constant n is an empirical parameter related to the adsorption intensity, and values of 'n' in the range of 1–10 indicate favorable adsorption.[89] The k_F values for the studied nanoparticle samples were 387.5 and 235.4 mg g^{-1} for CuO and ZnO NPs, respectively, indicating an enhanced adsorption capacity of copper oxide-based nanoparticles. This observation is in line with the data obtained from the Langmuir isotherm. For all studied samples, the values of the Freundlich constant (n) significantly exceed unity, indicating the feasibility of Pb(II) adsorption on the nanoparticle surface. The regression coefficients for the linear plots are close to unity, suggesting that the experimental adsorption data are in good agreement with the Freundlich adsorption isotherm.

Table 6 presents data on the sorption capacity of various nanosized sorbents for lead ions, as reported in earlier works. It is important to note that direct comparison of data from different studies can be challenging due to variations in factors influencing sorbent capacity, such as the mixing rate, pH and temperature. Nevertheless, the presented data indicate that biogenic ZnO and CuO nanoparticles synthesized using plant raw materials from SCR exhibit higher sorption capacity compared to existing analogues, rendering them promising materials for effective sorption removal of lead ions from aqueous media.

4. Conclusion

In conclusion, this study encompassed a comparative investigation of the wet combustion synthesis of the CuO and ZnO NPs, employing an environmentally friendly and non-toxic capping agent derived from *Serratula coronata* L. plant extract. Green chemistry principles were strictly followed, eliminating the use of aggressive organic solvents. The extraction method of SCR with ethyl alcohol and its aqueous-alcoholic solution was found to be technologically optimal, aligning with international standards of good manufacturing practice (GMP) in pharmaceutical production. The chemical composition of the extracts was analyzed, with particular emphasis on phenolic compounds and flavonoids, wherein flavonoids quercetin and rutin exhibited the highest content at the onset of the growing season in the water–ethanol extracts. The optimal period for collecting SCR plant material was identified to be from the third decade of May to the first half of June.

X-ray diffraction analysis of the NPs' crystalline structure and phase composition showed the formation of a single metal oxide phase in both cases, with monoclinic ZnO and cubic CuO phases exhibiting high purity and a narrow size distribution. Characterization techniques, such as XRD, SEM, XPS, TEM and EDS, confirmed the desired structure and composition of the synthesized NPs.

The sorption removal of lead ions from aqueous solutions using the biogenic NPs was thoroughly studied, and the impact of pH on the removal efficiency of Pb(II) was investigated. The adsorption behavior of Pb(II) on the surface of ZnO and CuO NPs was analyzed using Langmuir and Freundlich isotherm models, providing insights into the underlying mechanisms of the sorption process. Comparative analysis based on the mean-square deviations (R^2) indicated that the Freundlich model best describes the adsorption of Pb(II) on the surface of ZnO and CuO NPs. Furthermore, the adsorption kinetics of Pb(II) ions onto the NPs' surface was investigated using the Elovich rate equation, pseudo-first-order, and pseudo-second-order kinetic models. The results showed that the pseudo-second-order model provided a better fit for both NPs, suggesting that the rate-limiting step in the adsorption of Pb(II) ions can be attributed to chemical interactions between the metal ions and the functional groups present on the surface of NPs.

The findings of this study contribute to the understanding of the potential applications of biogenic NPs in the removal of lead ions from aqueous media, paving the way for further exploration and development of efficient sorption methods for water purification and environmental remediation.

Abbreviations

SCR	*Serratula coronata* L.
NPs	Nanoparticles
XRD	X-ray diffraction
XPS	X-ray photoelectron spectroscopy
SEM	Scanning electron microscopy
EDX	Energy dispersive X-ray analysis
TEM	Transmission electron microscopy
HPLC	High-performance liquid chromatography
FWHM	Full width at half maximum
Q_e	Amount of Pb(II) adsorbed by the unit mass of copper (mg g^{-1})
C_0	Feed Pb(II) concentration (mg L^{-1})
C_e	Concentration of Pb(II) in aliquots (mg L^{-1})
DC	Degree of crystallinity (%)
L	Average crystallite size (nm)
q_t	Adsorption capacity at time t (mg g^{-1})
α	Initial rate of the adsorption process, mg g^{-1} min^{-1}
β	Desorption constant (g $mmol^{-1}$)
R_a	Roughness of the composite (nm)
b	Constant related to the energy of adsorption (*i.e.*, Langmuir constant (L μg^{-1}))
C_e	Equilibrium concentration of adsorbate (mg L^{-1})
Q_0	Maximum monolayer coverage capacity (mg g^{-1})
k_F	Freundlich isotherm constant related to the adsorption capacity (μg g^{-1})

Author contributions

Conceptualization, A. A. M. and M. B.; methodology, A. A. M. and M. B.; validation, N. G. S, N. A. A. and A. N. A.; formal analysis, D. A. Zh., A. A. A., A. N. A., N. G. S., N. A. A.; investigation, N. G. S., A. A. A, B. S. T., D. T. S., A. M. Zh. and N. A. A.; writing – original draft preparation, A. A. M., N. G. S. and M. B.; writing – review and editing, N. G. S., M. B. and A. A. M.; supervision, M. B. and M. A. A.; project administration, A.

A. M.; funding acquisition, A. A. M. All authors have read and agreed to the published version of the manuscript.

Conflicts of interest

The authors declare no conflict of interest.

Acknowledgements

The research titled "Development and environmental applications of the biogenic catalysts and adsorbents from the Kazakhstan endemic plant sources" (grant no. AP09057856) was funded by the Ministry of Science and Higher Education of the Republic of Kazakhstan.

References

1 D. Sharma, S. Kanchi and K. Bisetty, *Arabian J. Chem.*, 2019, **12**, 3576–3600.
2 N. A. I. Md Ishak, S. K. Kamarudin and S. N. Timmiati, *Mater. Res. Express*, 2019, **6**, 112004.
3 H. K. Kehri, I. Zoomi, U. Singh, D. Pandey and D. Pandey, *J. Nanosci. Technol.*, 2019, **5**, 810–816.
4 S. Jadoun, R. Arif, N. K. Jangid and R. K. Meena, *Environ. Chem. Lett.*, 2021, **19**, 355–374.
5 M. Das and S. Chatterjee, in *Green Synthesis, Characterization and Applications of Nanoparticles*, Elsevier, 2019, pp. 265–301.
6 J. A. Kumar, T. Krithiga, S. Manigandan, S. Sathish, A. A. Renita, P. Prakash, B. S. N. Prasad, T. R. P. Kumar, M. Rajasimman, A. Hosseini-Bandegharaei, D. Prabu and S. Crispin, *J. Cleaner Prod.*, 2021, **324**, 129198.
7 A. Singh, P. K. Gautam, A. Verma, V. Singh, P. M. Shivapriya, S. Shivalkar, A. K. Sahoo and S. K. Samanta, *Biotechnol. Rep.*, 2020, **25**, e00427.
8 N. Zafar, A. Madni, A. Khalid, T. Khan, R. Kousar, S. S. Naz and F. Wahid, *Curr. Pharm. Des.*, 2020, **26**, 5844–5865.
9 L. Soltys, O. Olkhovyy, T. Tatarchuk and M. Naushad, *Magnetochemistry*, 2021, **7**, 145.
10 M. Dadkhah and J.-M. Tulliani, *Sensors*, 2022, **22**, 4669.
11 R. V. Bordiwala, *Results Chem.*, 2023, **5**, 100832.
12 S. P. Goutam and G. Saxena, in *Bioremediation for Environmental Sustainability*, Elsevier, 2021, pp. 623–636.
13 J. Singh, T. Dutta, K.-H. Kim, M. Rawat, P. Samddar and P. Kumar, *J. Nanobiotechnol.*, 2018, **16**, 84.
14 D. Aksu Demirezen, Y. Ş. Yıldız and D. Demirezen Yılmaz, *Environ. Nanotechnol., Monit. Manage.*, 2019, **11**, 100219.
15 H. Ali, E. Khan and I. Ilahi, *J. Chem.*, 2019, **2019**, 1–14.
16 K. Rehman, F. Fatima, I. Waheed and M. S. H. Akash, *J. Cell. Biochem.*, 2018, **119**, 157–184.
17 S. Mitra, A. J. Chakraborty, A. M. Tareq, T. Bin Emran, F. Nainu, A. Khusro, A. M. Idris, M. U. Khandaker, H. Osman, F. A. Alhumaydhi and J. Simal-Gandara, *J. King Saud Univ., Sci.*, 2022, **34**, 101865.
18 M. del R. M. Virgen, O. F. G. Vázquez, V. H. Montoya and R. T. Gómez, in *Heavy Metals*, InTech, 2018.
19 R. Singh, N. Gautam, A. Mishra and R. Gupta, *Indian J. Pharmacol.*, 2011, **43**, 246.
20 A. Alengebawy, S. T. Abdelkhalek, S. R. Qureshi and M.-Q. Wang, *Toxics*, 2021, **9**, 42.
21 N. A. A. Qasem, R. H. Mohammed and D. U. Lawal, *npj Clean Water*, 2021, **4**, 36.
22 M. L. Del Prado-Audelo, I. García Kerdan, L. Escutia-Guadarrama, J. M. Reyna-González, J. J. Magaña and G. Leyva-Gómez, *Front. Environ. Sci.*, 2021, **9**, 793765.
23 R. Kumar, P. Rauwel and E. Rauwel, *Processes*, 2021, **9**, 1379.
24 S. Azizi, M. Mahdavi Shahri and R. Mohamad, *Molecules*, 2017, **22**, 831.
25 A. Kumar, S. R. Shah, T. J. Jayeoye, A. Kumar, A. Parihar, B. Prajapati, S. Singh and D. U. Kapoor, *Front. Nanotechnol.*, 2023, **5**, 1175149.
26 A. V. Myagchilov, L. I. Sokolova, P. G. Gorovoy and A. A. Kechaikin, *Chem. Plant Raw Mater.*, 2020, 171–179.
27 V. N. Odinokov, I. V. Galyautdinov, D. V. Nedopekin, L. M. Khalilov, A. S. Shashkov, V. V. Kachala, L. Dinan and R. Lafont, *Insect Biochem. Mol. Biol.*, 2002, **32**, 161–165.
28 E. A. Konyaeva, O. G. Alentyeva and P. G. Mizina, *Farmaciya*, 2019, **68**, 27–30.
29 A. V. Myagchilov, L. I. Sokolova, P. G. Gorovoi and P. S. Dmitrenok, *Pharm. Chem. J.*, 2017, **51**, 119–123.
30 A. Kroma, M. Pawlaczyk, A. Feliczak-Guzik, M. Urbańska, D. Jenerowicz, A. Seraszek-Jaros, M. Kikowska and J. Gornowicz-Porowska, *Molecules*, 2022, **27**, 3471.
31 R. Mustarichie, T. Rostinawati, D. A. E. Pitaloka, N. M. Saptarini and Y. Iskandar, *Clin., Cosmet. Invest. Dermatol.*, 2022, **15**, 2391–2405.
32 M. Napierała, J. Nawrot, J. Gornowicz-Porowska, E. Florek, A. Moroch, Z. Adamski, A. Kroma, I. Miechowicz and G. Nowak, *Int. J. Environ. Res. Public Health*, 2020, **17**, 6453.
33 M. Báthori, I. Zupkó, A. Hunyadi, E. Gácsné-Baitz, Z. Dinya and P. Forgó, *Fitoterapia*, 2004, **75**, 162–167.
34 A. A. Mashentseva, N. A. Aimanova, N. Parmanbek, B. S. Temirgaziyev, M. Barsbay and M. V. Zdorovets, *Nanomaterials*, 2022, **12**, 3293.
35 A. A. Mashentseva, N. A. Aimanova, B. S. Temirgaziev, A. T. Zhumazhanova and B. I. Tuleuov, *Pet. Chem.*, 2020, **60**, 1141–1147.
36 A. N. Melentiyeva, V. S. Chuchalin and V. N. Burkova, *Bull. Sib. Med.*, 2011, **10**, 155–161.
37 R. M. Lamuela-Raventós, in *Measurement of Antioxidant Activity & Capacity*, John Wiley & Sons, Ltd, Chichester, UK, 2017, pp. 107–115.
38 A. Blainski, G. Lopes and J. de Mello, *Molecules*, 2013, **18**, 6852–6865.
39 S. A. Khan, F. Noreen, S. Kanwal, A. Iqbal and G. Hussain, *Mater. Sci. Eng., C*, 2018, **82**, 46–59.
40 L. S. Altynbaeva, A. A. Mashentseva, N. A. Aimanova, D. A. Zheltov, D. I. Shlimas, D. T. Nurpeisova, M. Barsbay, F. U. Abuova and M. V. Zdorovets, *Membranes*, 2023, **13**, 495.
41 J. Azmir, I. S. M. Zaidul, M. M. Rahman, K. M. Sharif, A. Mohamed, F. Sahena, M. H. A. Jahurul, K. Ghafoor, N. A. N. Norulaini and A. K. M. Omar, *J. Food Eng.*, 2013, **117**, 426–436.
42 A. Jovanovic, P. Petrovic, V. Đordjevic, G. Zdunic, K. Savikin and B. Bugarski, *Lek. Sirovine*, 2017, 45–49.

43 J. Dai and R. J. Mumper, *Molecules*, 2010, **15**, 7313–7352.
44 K. Ameer, H. M. Shahbaz and J.-H. Kwon, *Compr. Rev. Food Sci. Food Saf.*, 2017, **16**, 295–315.
45 S. Jain and M. S. Mehata, *Sci. Rep.*, 2017, **7**, 15867.
46 P. Kuppusamy, M. M. Yusoff, G. P. Maniam and N. Govindan, *Saudi Pharm. J.*, 2016, **24**, 473–484.
47 N. Sahu, D. Soni, B. Chandrashekhar, D. B. Satpute, S. Saravanadevi, B. K. Sarangi and R. A. Pandey, *Int. Nano Lett.*, 2016, **6**, 173–181.
48 S. Sukumar, A. Rudrasenan and D. Padmanabhan Nambiar, *ACS Omega*, 2020, **5**, 1040–1051.
49 A. S. Abdelbaky, T. A. Abd El-Mageed, A. O. Babalghith, S. Selim and A. M. H. A. Mohamed, *Antioxidants*, 2022, **11**, 1444.
50 A. Geremew, L. Carson, S. Woldesenbet, H. Wang, S. Reeves, N. Brooks, P. Saganti, A. Weerasooriya and E. Peace, *Front. Plant Sci.*, 2023, **14**, 1108186.
51 G. K. Prashanth, P. A. Prashanth, B. M. Nagabhushana, S. Ananda, G. M. Krishnaiah, H. G. Nagendra, H. M. Sathyananda, C. Rajendra Singh, S. Yogisha, S. Anand and Y. Tejabhiram, *Artif. Cells, Nanomed., Biotechnol.*, 2018, **46**, 968–979.
52 J. Osuntokun, D. C. Onwudiwe and E. E. Ebenso, *Green Chem. Lett. Rev.*, 2019, **12**, 444–457.
53 M. H. Kahsay, A. Tadesse, D. RamaDevi, N. Belachew and K. Basavaiah, *RSC Adv.*, 2019, **9**, 36967–36981.
54 M. M. Chikkanna, S. E. Neelagund and K. K. Rajashekarappa, *SN Appl. Sci.*, 2019, **1**, 117.
55 S. Talam, S. R. Karumuri and N. Gunnam, *ISRN Nanotechnol.*, 2012, **2012**, 1–6.
56 I. W. Okpashi, V. E. O. Bonaventure and C. U. C. Okoro, *J. Nanomed. Nanotechnol.*, 2015, **06**, 1–9.
57 A. A. Mashentseva, M. Barsbay, M. V. Zdorovets, D. A. Zheltov and O. Güven, *Nanomaterials*, 2020, **10**, 1552.
58 G. Greczynski and L. Hultman, *ChemPhysChem*, 2017, **18**, 1507–1512.
59 S. Evans, *Surf. Interface Anal.*, 1997, **25**, 924–930.
60 T. L. Barr and S. Seal, *J. Vac. Sci. Technol., A*, 1995, **13**, 1239–1246.
61 S. K. Shinde, D. P. Dubal, G. S. Ghodake and V. J. Fulari, *RSC Adv.*, 2015, **5**, 4443–4447.
62 M. A. Khan, N. Nayan, S. Shadiullah, M. K. Ahmad and C. F. Soon, *Nanomaterials*, 2020, **10**, 1298.
63 A. Molazemhosseini, L. Magagnin, P. Vena and C.-C. Liu, *J. Electroanal. Chem.*, 2017, **789**, 50–57.
64 R. P. Vasquez, *Surf. Sci. Spectra*, 1998, **5**, 262–266.
65 R. Al-Gaashani, S. Radiman, A. R. Daud, N. Tabet and Y. Al-Douri, *Ceram. Int.*, 2013, **39**, 2283–2292.
66 D. Barreca, A. Gasparotto, C. Maccato, C. Maragno and E. Tondello, *Surf. Sci. Spectra*, 2007, **14**, 19–26.
67 X. Yang, G. Xu and H. Yu, *Arabian J. Chem.*, 2019, **12**, 4142–4149.
68 A. Z. M. Badruddoza, Z. B. Z. Shawon, W. J. D. Tay, K. Hidajat and M. S. Uddin, *Carbohydr. Polym.*, 2013, **91**, 322–332.
69 S. E. Elaigwu, V. Rocher, G. Kyriakou and G. M. Greenway, *J. Ind. Eng. Chem.*, 2014, **20**, 3467–3473.
70 D. Mohan, H. Kumar, A. Sarswat, M. Alexandre-Franco and C. U. Pittman, *Chem. Eng. J.*, 2014, **236**, 513–528.
71 Á. Villabona-Ortíz, K. J. Figueroa-Lopez and R. Ortega-Toro, *Sustainability*, 2022, **14**, 3640.
72 F. Iazdani and A. Nezamzadeh-Ejhieh, *Environ. Sci. Pollut. Res.*, 2021, **28**, 53314–53327.
73 E. Leiva, C. Tapia and C. Rodríguez, *Water*, 2021, **13**, 2960.
74 A. Eleryan, U. O. Aigbe, K. E. Ukhurebor, R. B. Onyancha, M. A. Hassaan, M. R. Elkatory, S. Ragab, O. A. Osibote, H. S. Kusuma and A. El Nemr, *Environ. Sci. Pollut. Res.*, 2023, **30**, 69666–69682.
75 Z. He, S. Tian and P. Ning, *J. Rare Earths*, 2012, **30**, 563–572.
76 H. Moussout, H. Ahlafi, M. Aazza and H. Maghat, *Karbala Int. J. Mod. Sci.*, 2018, **4**, 244–254.
77 D. K. Singh, S. Mohan, V. Kumar and S. H. Hasan, *RSC Adv.*, 2016, **6**, 1218–1230.
78 S. Azizian, *J. Colloid Interface Sci.*, 2004, **276**, 47–52.
79 A. V. Russakova, L. S. Altynbaeva, M. Barsbay, D. A. Zheltov, M. V. Zdorovets and A. A. Mashentseva, *Membranes*, 2021, **11**, 116.
80 J.-P. Simonin, *Chem. Eng. J.*, 2016, **300**, 254–263.
81 M. V. Maslova, V. I. Ivanenko, N. Y. Yanicheva and N. V. Mudruk, *Int. J. Mol. Sci.*, 2020, **21**(2), 447.
82 L. K. Neudachina, A. Y. Golub, Y. G. Yatluk, V. A. Osipova, Y. A. Berdyugin, E. M. Gorbunova, L. V. Adamova, O. V. Koryakova and M. V. Kuznetsov, *Inorg. Mater.*, 2011, **47**, 435–441.
83 Y. S. Ho and G. McKay, *Water Res.*, 1999, **33**, 578–584.
84 E. Korzh and N. Klymenko, *Probl. Mod. Sci. Educ.*, 2017, **87**, 7–13.
85 T. A. Khan, S. A. Chaudhry and I. Ali, *J. Mol. Liq.*, 2015, **202**, 165–175.
86 N. Parmanbek, D. S. Sütekin, M. Barsbay, A. A. Mashentseva, D. A. Zheltov, N. A. Aimanova, Z. Y. Jakupova and M. V. Zdorovets, *Polymers*, 2022, **14**, 4026.
87 N. Ayawei, A. N. Ebelegi and D. Wankasi, *J. Chem.*, 2017, **2017**, 3039817.
88 P. K. Dutta, A. K. Ray, V. K. Sharma and F. J. Millero, *J. Colloid Interface Sci.*, 2004, **278**, 270–275.
89 P. C. Mishra and R. K. Patel, *J. Hazard. Mater.*, 2009, **168**, 319–325.
90 A. A. Farghali, M. Bahgat, A. Enaiet Allah and M. H. Khedr, *Beni-Suef Univ. J. Basic Appl. Sci.*, 2013, **2**, 61–71.
91 M. Verma, I. Tyagi, R. Chandra and V. K. Gupta, *J. Mol. Liq.*, 2017, **225**, 936–944.
92 P. K. Raul, S. Senapati, A. K. Sahoo, I. M. Umlong, R. R. Devi, A. J. Thakur and V. Veer, *RSC Adv.*, 2014, **4**, 40580–40587.
93 F. C. Christopher, S. Anbalagan, P. S. Kumar, S. R. Pannerselvam and V. K. Vaidyanathan, *IET Nanobiotechnol.*, 2017, **11**, 433–442.
94 Y. Tao, C. Zhang and T. Lü, *Appl. Sci.*, 2020, **10**(3), 948.